Modulational instability of two counterpropagating waves in an experimental transmission line

J. M. Bilbault, P. Marquié, and B. Michaux
Laboratoire de Physique de l'Université de Bourgogne, Phénomènes Non Linéaires, 6 Boulevard Gabriel, 21100 Dijon, France
(Received 19 July 1994)

We present experiments on the modulational instability of two counterpropagating waves, observed in an electrical transmission line. Our theoretical analysis leads to a set of two coupled nonlinear Schrödinger equations and predicts a partition of the linear spectrum into several regions with different behaviors. The unstable region, found in our previous study [Phys. Rev. E **49**, 828 (1994)] for a single wave, remains here unstable, but with a much larger growth rate. Moreover, two new unstable regions appear. Our experiments on the dynamics of the waves are in good agreement with the theoretical predictions.

PACS number(s): 03.40.Kf, 84.40.Mk

I. INTRODUCTION

Among the many fascinating effects due to nonlinearity, there is a great deal of interest in self-induced modulation of a plane wave [1], or modulational instability (MI), which occurs in nonlinear dispersive media. In this context, in a recent publication [2], we have investigated the MI conditions of a forward wave in an experimental transmission line and have shown that the linear spectrum can be divided into three different regions: between two modulationally stable regions, there exists a third region where spontaneous or induced MI can occur.

On the other hand, several theoretical or numerical papers have shown that, first, the modulational growth rate associated with a single unstable wave can be increased by the presence of a second wave [3,4], and second, two stable waves can become modulationally unstable in the other's presence [3,5,6]. However, to our knowledge, no experimental investigation has been reported. It is the purpose of this paper to present a quantitative analysis concerning MI for the superpostion of two counterpropagating waves in an experimental electrical network, with respect to the choice of the carrier frequency. We present in the second section the theoretical predictions based upon a set of two coupled nonlinear Schrödinger equations, which we compare in the third section with the experimental results. Then, the fourth section is devoted to some concluding remarks.

II. THEORETICAL STUDY

As in our previous paper [2], we consider a nonlinear network with N cells (see Fig. 1). Each cell contains two linear inductances, L_1 in series and L_2 in parallel, and a variable-capacitance diode (BB112), biased by a constant voltage V_0. Its capacitance $C(V_n)=C_0(1-\alpha V_n+\beta V_n^2)$ depends nonlinearly on the voltage V_n of the nth cell, with positive parameters C_0, α, and β. Neglecting in a first approximation the losses of the components, we easily derive from Kirchhoff's laws the system of nonlinear discrete equations (for $n=1,2,\ldots,N$)

$$(d^2V_n/dt^2)+\omega_0^2V_n+u_0^2(2V_n-V_{n+1}-V_{n-1}) =\alpha(d^2V_n^2/dt^2)-\beta(d^2V_n^3/dt^2)\ , \quad (2.1)$$

with $u_0^2=1/L_1C_0$ and $\omega_0^2=1/L_2C_0$. From (2.1), one gets the linear dispersion relation

$$\omega^2=\omega_0^2+4u_0^2\sin^2(k/2)\ , \quad (2.2)$$

which corresponds to a bandpass filter with a lower cutoff frequency $f_0=\omega_0/2\pi$ and an upper one, $f_{\max}=(\omega_0^2+4u_0^2)^{1/2}/2\pi$, introduced by the lattice effects.

We now focus on a particular case, that is, the coexistence of forward and backward propagating waves with the same angular frequency $f=\omega/2\pi$, and opposite wave numbers k and $-k$, but with their low amplitudes slowly varying in time and space with regard to the carrier waves. In order to use the reductive perturbation method [7], we introduce the independent multiple-scale variables $X_i=\varepsilon^i n$ and $T_i=\varepsilon^i t$, where $\varepsilon\ll 1$. Moreover, the solution of (2.1) is assumed to have the following form:

$$\begin{aligned}V_n(t)=&\varepsilon\mathcal{V}_{1+}(X_1,X_2,\ldots,T_1,T_2,\ldots)e^{i\theta+}\\&+\varepsilon^2\mathcal{V}_{2+}(X_1,X_2,\ldots,T_1,T_2,\ldots)e^{2i\theta+}\\&+\varepsilon\mathcal{V}_{1-}(X_1,X_2,\ldots,T_1,T_2,\ldots)e^{i\theta-}\\&+\varepsilon^2\mathcal{V}_{2-}(X_1,X_2,\ldots,T_1,T_2,\ldots)e^{2i\theta-}+\text{c.c.},\end{aligned} \quad (2.3)$$

where the carrier phases are $\theta+=kn-\omega t$ and $\theta-=-kn-\omega t$, and c.c. represents the complex conjugate. The second-harmonic terms $\mathcal{V}_{2\pm}$ are added to the

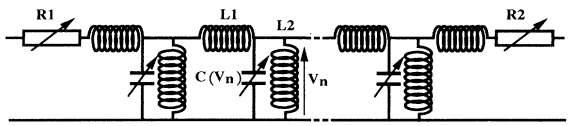

FIG. 1 Schematic representation of the experimental transmission line. The network is composed of 45 identical cells, with two linear inductances L1 and L2, and a variable-capacitance diode (BB112) of capacitance $C(V_n)$. Adjustable resistors R1 and R2 are used to minimize the reflected waves at both ends of the line.

fundamental ones $\mathcal{V}_{1\pm}$ in order to take the asymmetry of the variable-capacitance charge into account. However, as shown in our previous paper [2], the second-harmonic terms do not play any role when the carrier frequency f exceeds $f_{\max}/2$. Thus, in this case, they will not be considered.

Inserting (2.3) in (2.1) yields, after some standard calculations, a set of two coupled nonlinear Schrödinger (NLS) equations:

$$i\left[\frac{\partial \mathcal{V}_{1+}}{\partial T_2}+V_g\frac{\partial \mathcal{V}_{1+}}{\partial X_2}\right]+P\frac{\partial^2 \mathcal{V}_{1+}}{\partial X_1^2}+(Q_1|\mathcal{V}_{1+}|^2+Q_2|\mathcal{V}_{1-}|^2)\mathcal{V}_{1+}=0\ , \quad (2.4a)$$

$$i\left[\frac{\partial \mathcal{V}_{1-}}{\partial T_2}-V_g\frac{\partial \mathcal{V}_{1-}}{\partial X_2}\right]+P\frac{\partial^2 \mathcal{V}_{1-}}{\partial X_1^2}+(Q_1|\mathcal{V}_{1-}|^2+Q_2|\mathcal{V}_{1+}|^2)\mathcal{V}_{1-}=0\ , \quad (2.4b)$$

where the group velocity $V_g=d\omega/dk=u_0^2\sin k/\omega$ and the group velocity dispersion

$$P=(d^2\omega/dk^2)=(u_0^2\cos k-V_g^2)/2\omega$$

is calculated from (2.2), while the nonlinear coefficients Q_1 and Q_2 are, respectively,

$$Q_1=Q_1'=\omega\left[\frac{3\beta}{2}-\frac{4\alpha^2\omega^2}{3\omega_0^2+16u_0^2\sin^4 k/2}\right],\quad Q_2=3\beta\omega \quad \text{for } f<f_{\max}/2\ , \quad (2.5a)$$

$$Q_1=Q_1''=3\beta\omega/2\ ,\quad Q_2=3\beta\omega \quad \text{for } f>f_{\max}/2\ . \quad (2.5b)$$

Physically, the set of two slow variables ($T=T_2$ and $X=X_1=X_2$) is sufficient to describe the evolution of the envelopes, which corresponds to letting ε tend to unity.

We now turn our attention to modulation instability (MI). Equations (2.4) admitting plane wave solutions

$$\mathcal{V}_{1+}=\mathcal{V}_{1-}=\mathcal{V}_0\exp[i(Q_1+Q_2)\mathcal{V}_0^2T]\ ,$$

we consider small amplitude and phase perturbations (respectively $a_\pm$ and $b_\pm$), such as

$$\mathcal{V}_{1\pm}=(\mathcal{V}_0+a_\pm+ib_\pm)\exp[i(Q_1+Q_2)|\mathcal{V}_0|^2T]\ . \quad (2.6)$$

Inserting (2.6) in (2.4) and assuming that $a_\pm$ and $b_\pm$ are of the form $\exp i[K(X\pm V_gT)-i\sigma T]+\text{c.c.}$ yields a set of four equations in $a_\pm$ and $b_\pm$, whose determinant must be zero, that is,

$$\sigma^2=-P^2K^4+2PK^2|\mathcal{V}_0|^2(Q_1\pm Q_2)\ . \quad (2.7)$$

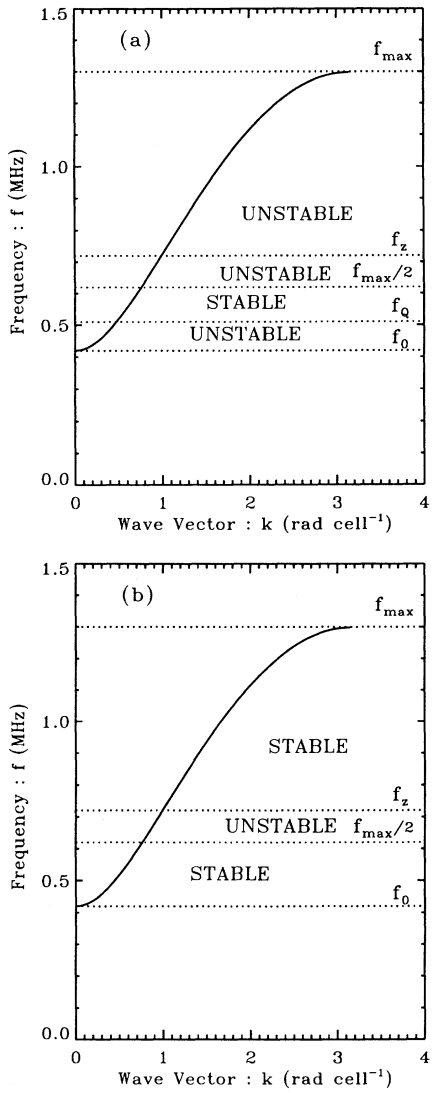

FIG. 2. Partition of the linear spectrum (f_0,$f_{\max}$) of the line into several regions concerning the stability of two counterpropagating waves (a), and for a single propagating wave (b).

MI appears when (2.7) leads to positive σ^2 solutions. Setting f_z, the zero dispersion frequency, and f_Q the lower frequency, where $Q_1'+Q_2$ becomes zero, while Q_2 is always positive, we have to consider four carrier frequency bands, due to the signs of the coefficients of (2.7). As summarized in Table I, three of these regions are modula-

TABLE I. Partition of the linear spectrum into four regions concerning modulational instability (MI) or stability (no MI). The coefficients of Eq. (2.7) are given with their signs. Note that Q_2 is always positive. In the MI regions, the maximum instability is obtained for the wave number K_{opt}, depending on the plane wave amplitude $|\mathcal{V}_0|$.

Region I	Region II	Region III	Region IV
$f_0<f<f_Q$	$f_Q<f<f_{\max}/2$	$f_{\max}/2<f<f_z$	$f_z<f<f_{\max}$
$P>0$, $Q_1=Q_1'$	$P>0$, $Q_1=Q_1'$	$P>0$, $Q_1=Q_1''$	$P<0$, $Q_1=Q_1''$
$Q_1'+Q_2>0$	$Q_1'+Q_2<0$	$Q_1''+Q_2>0$	$Q_1''-Q_2<0$
MI	no MI	MI	MI
$K_{\text{opt}}=$ $[(Q_1'+Q_2)\lvert\mathcal{V}_0\rvert^2/P]^{1/2}$		$K_{\text{opt}}=$ $[(Q_1''+Q_2)\lvert\mathcal{V}_0\rvert^2/P]^{1/2}$	$K_{\text{opt}}=$ $[(Q_1''-Q_2)\lvert\mathcal{V}_0\rvert^2/P]^{1/2}$

tionally unstable in the Benjamin-Feir sense [1], if the wave number K of the perturbation belongs to the instability domain, that is, $0<K<\sqrt{2}K_{\text{opt}}$. The perturbation wave number K_{opt}, corresponding to the maximum instability, is given by Table I. Using $F=V_gK/2\pi$ and Eqs. (2.5)–(2.7), we easily get the maximum growth rate and the relevant perturbation frequency, which are, e.g., for $f_{\max}/2<f<f_z$, that is, in region III,

$$\sigma_2=\tfrac{9}{2}\beta\omega|\mathcal{V}_0|^2\ ,\quad (F_{\text{opt}})_2=V_g(9\beta\omega|\mathcal{V}_0|^2/2P)^{1/2}/2\pi\ . \tag{2.8}$$

Table I also shows that, for a carrier frequency in region II, that is, for $f_Q<f<f_{\max}/2$, no instability is theoretically expected. For the sake of clarity, the different regions of MI occurrence are also displayed in Fig. 2(a) with respect to the dispersion curve.

These results can be compared to those obtained for a single propagating wave, as shown in Fig. 2(b). More precisely, for a single wave, we have shown that only the frequency band $f_{\max}/2<f<f_z$ (that is, region III of Table I) presents MI, the maximum growth rate and the relevant perturbation frequency being respectively, given by

$$\sigma_1=\tfrac{3}{2}\beta\omega|\mathcal{V}_0|^2\ ,\quad (F_{\text{opt}})_1=V_g(3\beta\omega|\mathcal{V}_0|^2/2P)^{1/2}/2\pi\ . \tag{2.9}$$

Here, one can remark that the $(F_{\text{opt}})_2$ and σ_2 are respectively $\sqrt{3}$ and 3 times larger than $(F_{\text{opt}})_1$ and σ_1, according to a large number of theoretical studies [3,4] devoted to different physical systems.

Finally, when we compare Figs. 2(a) and 2(b), we observe that, in addition to region III, which is unstable for both a single wave and the superposition of two counterpropagating waves, the presence of the backward wave gives rise to two other unstable bands, regions I and IV, while region II always remains stable.

III. EXPERIMENTAL RESULTS

The experimental line is the same as in our previous paper, with $N=45$ identical cells. The variable-capacitance diode (BB 112) is biased by $V_0=2$ V, which gives $C_0=320$ pF, $\alpha=0.21\ \text{V}^{-1}$, and $\beta=0.02\ \text{V}^{-2}$. The linear inductances are $L_1=220\ \mu$H and $L_2=470\ \mu$H. Under these conditions, one has the characteristic frequencies $f_0=435$ kHz, $f_Q=520$ kHz, $f_z=720$ kHz and $f_{\max}=1280$ kHz, with a relative precision of about 5%. A plane wave is launched at both ends of the line, which present adjustable resistors in order to minimize the parasitic reflected waves. The wave forms are observed and stored by using a numerical oscilloscope (Lecroy 9450) with fast-Fourier-transform processing.

We first investigate the stability of the superposition of two counterpropagating waves with the same frequency and amplitude, say $2|\mathcal{V}_0|=1.1$ V, near the center of the line, which is at cell 22, and over the whole frequency range $f_0<f<f_{\max}$. No instability is experimentally detected for 500 kHz$\cong f_Q<f<620$ kHz$\cong f_{\max}/2$, which agrees rather well with the above theoretical predictions. In the other frequency bands an instability develops, leading to a self-modulation of the resulting wave, with a modulation frequency appearing spontaneously from the electrical noise spectrum. The oscillograms of Fig. 3 represent an example of spontaneous MI, for $f=470$ kHz that is in region I, the experimental modulation frequency $F_{\text{exp}}=20$ kHz being given by the Fourier spectrum. Measuring also $V_g=1.65$ cells/μs and using $K=(2\pi/V_g)F$, one gets an experimental value for the perturbation wave number, giving the maximum of MI, $K_{\text{exp}}=0.076$ rad cell^{-1}, which is very close to the theoretical one, $K_{\text{opt}}=0.080$ rad cell^{-1}, provided by Table I. Note that the theoretical optimum perturbation frequency F_{opt} is then 21 kHz.

Then, we consider the instability that can be induced by a coherent and weak external modulation. We launch the same sinusoidal wave, with $f=470$ kHz and $2|\mathcal{V}_0|=1.1$ V, slightly amplitude modulated (10%) at both ends of the line, and we remark that the modulation rate of the resulting wave, at cell number $n=22$, varies with the envelope frequency. It becomes maximum (50%) when the modulation frequency is about 18 kHz. This value agrees quite well with that found for the spontaneous MI (20 kHz), and with the theoretical one, $F_{\text{opt}}=21$ kHz.

Next, we consider at the 22nd cell the superposition of forward and backward propagating waves, but the carrier frequency $f=800$ kHz lies now in region IV, and the amplitude is $2|\mathcal{V}_0|=0.6$ V. The initial modulation rate (20%) increases up to 45%, when the modulation frequency is about 105 kHz. This value is in good agreement with the theoretical one, $F_{\text{opt}}=115$ kHz calculated from Table I and for region IV.

Let us now consider the case of a carrier frequency lying in region III. First, a single wave with $f=670$ kHz, $2|\mathcal{V}_0|=0.17$ V and slightly (25%) amplitude modulated (see Fig. 4) is launched at the left end of the line, the right one being carefully matched with a load resistance to

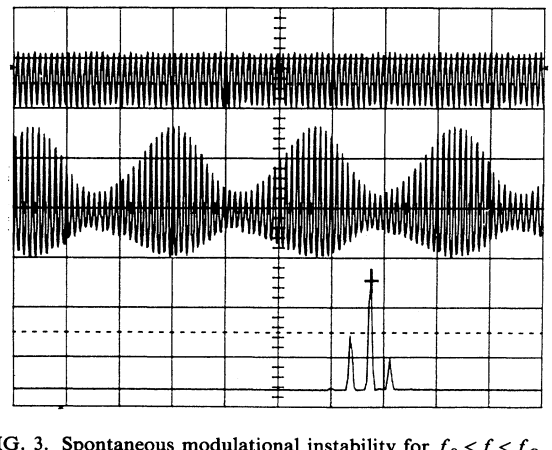

FIG. 3. Spontaneous modulational instability for $f_0<f<f_Q$. Representation (above) of the initial plane wave with $f=470$ kHz and a constant amplitude $2|\mathcal{V}_0|=1.1$ V, which is launched at both ends of the line (abscissa: 20 μs/div.; ordinate: 2 V/div.). The other oscillograms correspond respectively to the observation at cell $n=22$ of the self-modulated wave train (abscissa: 20μs/div.; ordinate: 2 V/div.) and the relevant Fourier spectrum; the carrier frequency is 470 kHz (central peak) with an amplitude of 1.1 V. The sidebands due to modulation are $\pm$20 kHz away (ordinate: 0.5 V/div.).

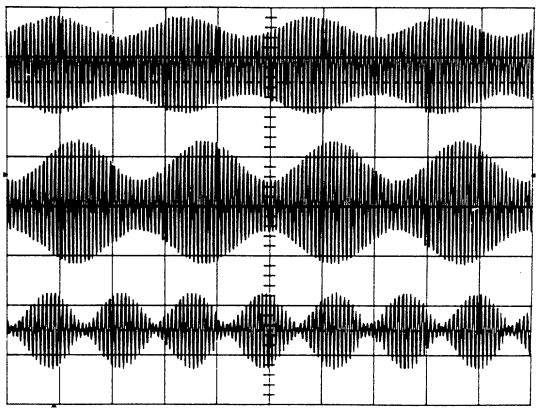

FIG. 4. Induced modulational instability for $f_{max}/2 < f < f_z$. The initial plane wave supplied by the generator (above, abscissa: 20 μs/div., ordinate: 0.5 V/div.), with $f = 670$ kHz, $2|V_0| = 0.17$ V and a 25% modulation rate, is launched either at the left end or at both ends of the line. The middle oscillogram represents the observation at cell $n = 22$ of the single wave, whose modulation rate is then maximum (43%) for $F = 20.5$ kHz (abscissa: 20μs/div.; ordinate: 0.2 V/div.). The last oscillogram represents, at the same cell number, the superposition of the two counterpropagating waves; the modulation rate is now 68% and $F = 38$ kHz (abscissa: 20 μs/div.; ordinate: 0.2 V/div.).

minimize the reflected wave. As observed previously, this modulation becomes maximum (43%, see Fig. 4) at cell number $n = 22$, when the modulation frequency is set to 20.5 kHz, a value very close to the theoretical one, $(F_{opt})_1 = 20$ kHz, predicted by Eq. (2.9). Launching now the same wave at both ends of the line, we observe the superposition of forward and backward waves again at the 22nd cell; the modulation becomes maximum (68%, see Fig. 4) for a modulation frequency $F = 38$ kHz. The agreement with Eq. (2.8), giving a theoretical frequency $(F_{opt})_2 = 35$ kHz, is rather good, and we effectively retrieve $(F_{opt})_2 = \sqrt{3}(F_{opt})_1$. We also note that the modulation rate is quite larger for the superposition of two counterpropagating waves than for a single one, which qualitatively confirms the theoretical prediction about the increase of the maximum growth rate. It is important to remark, that in our experiments the carrier frequency remains always fixed. Thus, the effects we report here are purely nonlinear.

Finally, no variation of the modulation rate is experimentally found when we launch a slightly modulated wave with a carrier frequency f, with 500 kHz $< f <$ 620 kHz, that is in region II. This confirms that this frequency band is modulationally stable, as predicted by the theoretical study.

IV. CONCLUSION

In this paper, we have studied the superposition of two counterpropagating waves with the same frequency in a nonlinear electrical transmission line. We have shown that the evolution of their slowly varying amplitudes can be modeled by two coupled NLS equations. Then, we have calculated theoretically the modulational instability conditions, namely the maximum growth rate and the corresponding perturbation wave number. From this analysis, four different frequency regions can be predicted: in addition to region III, already unstable for a single wave, two other regions, i.e., regions I and IV, become unstable due to the presence of the counterpropagating wave.

Next, we have experimentally found the different regions predicted by the theory. In regions I, III, and IV, spontaneous or induced modulational instability occurs, and the results agree very well with the theory. Moreover, we have effectively observed in region III that the maximum growth rate is larger for two counter propagating waves than for either wave alone, with the corresponding modulation frequencies in the ratio of $\sqrt{3}$. In addition, no instability is detected in region II, that is, for 500 kHz $< f <$ 620 kHz.

Therefore, the presence of a counterpropagating wave drastically modifies the dynamics of the incident wave. We must emphasize here that our first motivation was to verify fundamental features of MI appearance in nonlinear transmission systems. Thus, a low frequency range has been chosen for practical convenience, so that the voltage wave forms can be directly measured with oscilloscope probes. Potential applications can, however, be considered with higher frequencies, e.g., at microwave frequencies, where nonlinear transmission lines have been constructed to generate high frequency [8] or high-power [9] pulses. MI may then behave as parasites and must be avoided. For these practical applications, we can predict that the useful frequency band will be restricted due to any reflected wave with respect to the case of a single wave.

[1] T. B. Benjamin and T. E. Feir, J. Fluid Mech. **27**, 417 (1967).
[2] P. Marquié, J. M. Bilbault, and M. Remoissenet, Phys. Rev. E **49**, 828 (1994).
[3] C. J. McKinstrie and G. G. Luther, Phys. Scr. **30**, 31 (1990). and references therein.
[4] D. Barday and M. Remoissenet, Phys. Rev. B **43**, 7297 (1991).
[5] G. P. Agrawal, P. L. Baldeck, and R. R. Alfano, Phys. Rev. A **39**, 3406 (1989).
[6] G. P. Agrawal, Phys. Rev. Lett. **59**, 880 (1987).
[7] T. Taniuti and N. Yajima, J. Math. Phys. **10**, 1369 (1969).
[8] E. Carmann, K. Giboney, M. Case, M. Kamegawa, R. Yu, K. Abe, M. Rodwell, and J. Franklin, IEEE Microwave Guided Wave Lett. **1**, 28 (1991).
[9] H. Ikezi, S. S. Wojtowicz, R. E. Waltz, J. S. de Grassie, and D. R. Baker, J. Appl. Phys. **64**, 3277 (1988).